



## ARTICLE

# A Stable, Reliable, Cost-Effective Technique Route for Ni Detection in Industrial Wastewater via a Microfluidic Paper-Based Platform

Xiuxia Li <sup>1,2</sup> , Qing'er Yao <sup>3</sup>, Jiangyue Bai <sup>1,2</sup>, Zihang Wang <sup>3</sup>, Xiaolu Xiong <sup>4</sup>, Zifan Ning <sup>1</sup>, Songhe Liu <sup>1</sup>, Shiqi Xu <sup>1,2</sup>, Chunpan Zhang <sup>1,2</sup>, Yujiu Jiang <sup>1,2</sup>, Mingxu Chu <sup>5</sup>, Yanbo Yang <sup>1,2\*</sup>, Dong Jiang <sup>5\*</sup>, Junfeng Han <sup>1,2\*</sup> 

<sup>1</sup>Centre for Quantum Physics, Key Laboratory of Advanced Optoelectronic Quantum Architecture and Measurement (MOE), School of Physics, Beijing Institute of Technology, Beijing 100081, China

<sup>2</sup>International Center for Quantum Materials, Beijing Institute of Technology, Zhuhai 519000, China

<sup>3</sup>Yangtze Delta Region Academy of Beijing Institute of Technology, Jiaxing 314019, China

<sup>4</sup>The Analysis & Testing Center, Beihang University, Beijing 100191, China

<sup>5</sup>Guangdong Xindayu Environmental Technology Co., Ltd., Shenzhen 510000, China

## ABSTRACT

Nickel (II) as one of the primary categories of heavy metals can lead to serious health problems if achieving the critical levels in the water. Thus, it is vital to propose a stable, reliable, and economical approach for detecting Ni ions. The microfluidic paper-based analytical devices (μPADs) are potential candidates for the detection of water quality parameters including pH, heavy ions, nitrite and so on. However, it suffers from a huge error caused by the environment and artificial mistakes. In this study, we proposed an improved technique route to increase the stability and reliability of microfluidic paper-based analytical devices. The main technique points include a stable light source, a matched camera, improved reliability of the devices, and effective calculated methods. Finally, we established 15 standard curves that could be used to

### \*CORRESPONDING AUTHOR:

Yanbo Yang, Centre for Quantum Physics, Key Laboratory of Advanced Optoelectronic Quantum Architecture and Measurement (MOE), School of Physics, Beijing Institute of Technology, Beijing 100081, China; International Center for Quantum Materials, Beijing Institute of Technology, Zhuhai 519000, China; Dong Jiang, Guangdong Xindayu Environmental Technology Co., Ltd., Shenzhen 510000, China; Junfeng Han, Centre for Quantum Physics, Key Laboratory of Advanced Optoelectronic Quantum Architecture and Measurement (MOE), School of Physics, Beijing Institute of Technology, Beijing 100081, China; International Center for Quantum Materials, Beijing Institute of Technology, Zhuhai 519000, China; Email: yyb66@bit.edu.cn (Y.Y.); jd689@139.com (D.J.); pkuhfj@bit.edu.cn (J.H.)

### ARTICLE INFO

Received: 15 January 2025 | Revised: 5 February 2025 | Accepted: 13 February 2025 | Published Online: 2 April 2025

DOI: <https://doi.org/10.30564/jees.v7i4.8433>

### CITATION

Li, X., Yao, Q., Bai, J., et al., 2025. A Stable, Reliable, Cost-Effective Technique Route for Ni Detection in Industrial Wastewater via a Microfluidic Paper-Based Platform. *Journal of Environmental & Earth Sciences*. 7(4): 280–290. DOI: <https://doi.org/10.30564/jees.v7i4.8433>

### COPYRIGHT

Copyright © 2025 by the author(s). Published by Bilingual Publishing Group. This is an open access article under the Creative Commons Attribution-NonCommercial 4.0 International (CC BY-NC 4.0) License (<https://creativecommons.org/licenses/by-nc/4.0/>).

detect nickel ions and obtained uniform colorimetric results with reliability and repeatability. With those improvements, the relative errors for the five types of real water samples from the Zhongshan industrial parks were reduced to 0.26%, 14.78%, 24.20%, 50.29% and 3.53%, respectively. These results were conducive to exploring this technique for the detection of nickel ions in wastewater from the Zhongshan industrial parks. The results demonstrated that the above technique route is promising for the detection of other heavy metal ions in industrial effluent.

**Keywords:** Nickel Detection; Industrial Wastewater Detection; Microfluidic Paper-Based Chips; Analytical Device

## 1. Introduction

The water environment has been greatly influenced by industrial effluents over the last few decades on a worldwide scale<sup>[1]</sup>. When the concentration of nickel ions in water exceeds the standard, it will inhibit the photosynthesis and respiration of aquatic plants, affect their growth and reproduction, and consequently disrupt the entire aquatic food chain<sup>[2, 3]</sup>. Regarding the impact on human health, excessive nickel ions in water will get into the human body and preferentially accumulate in vital organs such as the liver, kidneys, lungs, and bones<sup>[4, 5]</sup>. That will also damage the urinary system, affecting the normal metabolism and excretion functions of the kidneys and causing kidney diseases and cancer<sup>[6–8]</sup>.

The current main technology, atomic absorption spectroscopy (AAS), is a well-known and commonly used analytical technique in scientific and industrial fields<sup>[9, 10]</sup>. Despite its high-accuracy elemental analysis, AAS has its drawbacks, such as high costs, limited accessibility, and a time-consuming process<sup>[11, 12]</sup>. Other methods include inductively coupled plasma mass spectrometry (ICP-MS) and electrochemical analysis. ICP-MS features rapid detection speed and high sensitivity, enabling the measurement of trace amounts of nickel<sup>[13, 14]</sup>. But it is expensive and needs professional operators. Electrochemical analysis, such as anode stripping voltammetry, determines the concentration based on the electrochemical behavior of nickel ions on the electrode surface. The equipment is portable, and the analysis is fast, making it suitable for on-site detection<sup>[15]</sup>. The disadvantage is that the accuracy is easily influenced by the sample matrix. In summary, traditional heavy metal detection methods suffer from issues such as high-cost instruments, complex operations, cumbersome sample preparation procedures, and the requirement for professional expertise<sup>[16]</sup>. The development of a stable, reliable, low-cost technique

route is still the key to solving the problem of nickel pollution in industrial wastewater.

One potential technology is microfluidic paper-based analysis devices ( $\mu$ PADs), which were launched in 2007<sup>[17, 18]</sup>. In recent years, an increasing interest in microfluidic paper-based chips ( $\mu$ PCs) for water quality detection has been reported<sup>[19–21]</sup>. Microfluidic paper-chip technology, with its advantages of rapidity, low cost, simplicity, and reliability, has emerged as a new option for the detection of heavy metal ions in industrial wastewater<sup>[22–31]</sup>. Especially after being fabricated with inexpensive and environmentally friendly materials, its production efficiency has been enhanced<sup>[12]</sup>. The detection techniques of microfluidic paper-chip technology are diverse, covering colorimetry, absorbance-based detection, electrochemical detection, fluorescence detection, etc. The research focus lies in improving these techniques to lower the limit of detection<sup>[13]</sup>. Meanwhile, the application of novel materials and scalable microfabrication methods in the manufacturing of microfluidic and lab-on-chip devices has provided a direction for the research on the detection of heavy metal ions in industrial wastewater using microfluidic paper chips<sup>[32]</sup>. In addition, by using a smartphone to capture the image for color analyses, the detection process becomes faster and easier to operate<sup>[33–38]</sup>. However, the detection stability and reliability are limited by the quality of paper-based chips and the work condition of the image capture system, which are quite important for the detection of real industrial effluent. In addition, the strong acidity of industrial wastewater is also a factor that leads to the difficulty of color development of paper-based chips.

This study aims to improve the stability and reliability of  $\mu$ PCs themselves and to provide ideas for practical industrial wastewater detection. It has been successfully applied to the detection of wastewater in industrial parks by using a confined dark space, a stable light source, an industrial camera with fixed parameters to capture images, and by developing

a method to quantify color rendering uniformity.

## 2. Materials and Methods

### 2.1. Reagents

The standard solutions of nickel sulfate solution were  $1000 \text{ mg L}^{-1}$ ,  $900 \text{ mg L}^{-1}$ ,  $800 \text{ mg L}^{-1}$ ,  $700 \text{ mg L}^{-1}$ ,  $600 \text{ mg L}^{-1}$ ,  $500 \text{ mg L}^{-1}$ ,  $400 \text{ mg L}^{-1}$ ,  $300 \text{ mg L}^{-1}$ ,  $200 \text{ mg L}^{-1}$ ,  $100 \text{ mg L}^{-1}$ , and  $50 \text{ mg L}^{-1}$  respectively. Sodium fluoride solution and disodium hydrogen phosphate-citrate buffer were prepared by dissolving sodium fluoride (Aladdin), anhydrous disodium hydrogen phosphate (Meryer), and citrate (Aladdin) in Milli-Q water, respectively. A dimethylglyoxime solution was prepared by dissolving dimethylglyoxime (Aladdin) with acetone (Tianjin Fuyu). In addition, an acetic acid solution was prepared by the dissolution of glacial acetic acid (Tianjin Fuyu) into Milli-Q water. The pH of the concentrated ammonia solution was measured by the pH meter (Aladdin), which was 12.6 in all experiments. Five types of wastewater, pretreatment of raw water (sample①), mixed discharge raw water (sample②), nickel raw water (sample③), chemical nickel raw water (sample④), and composite raw water (sample⑤), were taken from the Zhongshan Huafeng electroplating factory. Mixed chromogenic agents I contained  $200 \mu\text{L}$  sodium fluoride ( $0.5 \text{ M}$ ),  $500 \mu\text{L}$  dimethylglyoxime ( $40 \text{ mg ml}^{-1}$ ), and  $350 \mu\text{L}$  disodium hydrogen phosphate-citrate buffer at different pH ( $\text{pH} = 8.0, 7.8, 7.6, 7.4, 7.2, 7.0, 6.8, 6.6$ ). Mixed chromogenic agents II contained  $200 \mu\text{L}$  sodium fluoride ( $0.5 \text{ M}$ ),  $500 \mu\text{L}$  dimethylglyoxime ( $40 \text{ mg ml}^{-1}$ ),  $100 \mu\text{L}$  acetic acid solution ( $6.3 \text{ M}$ ) and  $250 \mu\text{L}$  ammonia solution ( $\text{pH} = 12.6$ ).

### 2.2. Chip Design and Fabrication

The pattern of the chip comprised a blank zone ( $6 \text{ mm}$  diameter) right in the middle, 6 detection zones ( $6 \text{ mm}$  diameter), and 6 channels ( $2.8 \times 2 \text{ mm}$ ) to connect the zones (Figure 1). That pattern was printed onto Whatman grade I qualitative filter paper using a Xerox ColorQube 8580 wax printer (UK). The printed chip was melted at  $150 \text{ }^{\circ}\text{C}$  for  $115 \text{ s}$  using a hot plate (Kaisi 818, China), forming three-dimensional hydrophobic barriers as the wax melted into the paper. The back of the chip was sealed with PET hot laminating film (GD-09MP) to prevent the leakage of the solution

through the paper during the experiment. More details can be found in our previous work<sup>[39]</sup>.

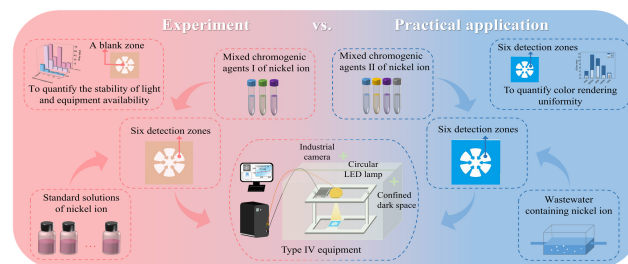


**Figure 1.** Establishment of standard curves and detection of industrial wastewater.

### 2.3. Colorimetric Detection

The detection process is shown in Figure 1. A confined dark space was used to exclude the influence of external light, and a circular LED lamp (Chao Yan furniture franchise store) was used to provide stable and uniform illumination. An industrial camera (DW1200-2.8 mm, no distortion,  $130$  degrees) was used to capture images. In addition, the data measured by the A3 atomic absorption spectrophotometer (Beijing Puxi General Instrument Co., LTD) was used as the standard for nickel ion concentration in wastewater.

### 2.4. Image Analysis

For colorimetric analysis, the paper-based chips were captured in the JPG format at  $96 \text{ dpi}$  by VideoCap of industrial cameras after the optimal reaction time. The images were processed using ImageJ to determine the color intensity of six detection zones and the blank zone. We chose gray values instead of RGB components. By drawing the relationship between color intensity and nickel ion concentration, the linear regression equation of different mixed chromogenic agents was obtained.

We proposed an effective technique route to improve the stability and reliability of the detection results based on  $\mu\text{PCs}$ . First, we improved the design and fabrication of chips for Ni detection by developing a method to quantify color rendering uniformity. Second, we developed a suitable system composed of a stable light source, a confined dark space, and an industrial camera for identifying the color of the reaction with Ni. Then, we established standard curves with different pH values to deal with the complexity of industrial wastewater. Finally, we checked the developed system by

detecting five different types of real water samples containing nickel ions from the Zhongshan Huafeng electroplating factory using our methods.

### 3. Results and Discussion

#### 3.1. Quantification of Color Rendering Uniformity

To improve the performance of our chips, we first optimized the volumes of mixed chromogenic agents (5.0–13  $\mu\text{L}$ ), the nickel ion volumes (1.5–2.5  $\mu\text{L}$ ) and reaction times (0–10 mins) on the color intensity response (**Figure 2**).

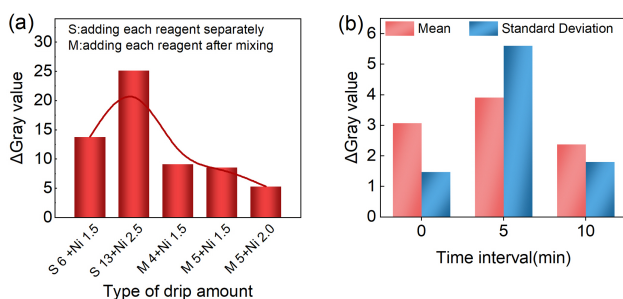


**Figure 2.** Chip optimization for Ni detection. (a) Five types of drops of chromogenic agents and standard solution; (b) Three types of time intervals.

First of all, it was vital to note that the volume conditions of mixed chromogenic agents and nickel ions were explored in the device. The “S” in **Figure 2a** stands for adding each reagent separately, and “M” stands for adding each reagent after mixing. The method to quantitatively evaluate whether the color rendering was uniform was to calculate the maximum value of the difference between the gray values of each detection area, namely  $\Delta\text{gray}$  value. The specific drip method of reagent is shown in the caption of **Figure S1**. When the reagent was added separately, the paper-based chip was prone to an uneven surface and took a long time to dry because it bore more liquid. Irrespective of whether the reagents were dropped separately or mixed, solutions of 0.5, 1, and 1.5  $\mu\text{L}$  could only diffuse to within half of the detection zones, resulting in uneven mixing of the chromogenic agents and inadequate reaction with the liquid to be measured. **Figure S1** shows the chips after the color development of five types of drops. The first four types of drip amounts all appeared with the phenomenon that the edge was darker than the center, and this uneven color rendering

would bring great error to the subsequent extraction of gray value. It could be seen from **Figure 2a** that M 5+Ni 2.0 had the smallest  $\Delta\text{gray}$  value, so this condition was eventually adopted.

Furthermore, the optimal reaction time was explored with the above conditions of M 5+Ni 2.0. **Figure S2** shows the color development results under different time intervals of mixed chromogenic agents and nickel ion solution. It could be seen that the color difference between the edge and the middle was large and uneven when the mixed chromogenic agents were dropped twice continuously. Two 2.5  $\mu\text{L}$  aliquots of mixed chromogenic agents and nickel ion solution were dropped at five-minute intervals, then the color was relatively uniform. The most uniform color development was found when time intervals were ten minutes. The standard of color uniformity was the maximum value of the difference between the gray values of each detection area ( $\Delta\text{gray}$  value). **Figure 2b** shows the average value of the  $\Delta\text{gray}$  value in blue and its standard deviation in pink. It could be seen that the  $\Delta\text{gray}$  value was the smallest when the time interval was 10 minutes, which means the color development was the most uniform, and the standard deviation was small, indicating good stability. Eventually, we chose 10 minutes as the best reaction time between the two aliquots of mixed chromogenic agents and the solution to be tested. In addition, a longer time cannot give better results, while it costs more time to give the results.

#### 3.2. Improvements of the Analysis Equipment for Image Capturing

To minimize the error caused by the light intensity, it was crucial that the light and dark degree of the environment was consistent and the light intensity was stable. If the chip was directly exposed to outdoor or indoor natural light, when the camera was at different times or different geographical locations, the environmental light changes would have a great impact on the gray value of the chip. The error caused by the above changes was much larger than the difference in gray values caused by the concentration gradient. Based on this idea, we made many improvements to the shooting equipment, of which the most frequently used were the following five. Given this, we created a confined dark space with an exclusive light source as the shooting environment that could minimize the impact of ambient light. Six detection zones



could balance the light intensity difference at different locations on the paper-based chips, which were re-shot more than five times to eliminate the systematic error. During this process, the performance of five types of equipment was tested.

Thus, we optimized the light source and image capturing as shown in **Figure 3a**. We tested the circular LED and long LED as the light source, respectively. The circular LED can offer a more uniform and stable light on the chips. We also optimized the parameters of the camera. To compare the performance of the four improved equipment, the mean value, the maximum difference, the ratio of the maximum difference to the mean, and the standard deviation of the gray value of the blank zone were calculated, as shown in **Figure 3b**. The blank zone of each paper-based chip was not dripped with any reagent, so its gray value could be used as a criterion of whether the light was stable. The maximum difference ( $\Delta$ ) and standard deviation ( $\sigma$ ) of the gray value of the blank zone could reflect the stability of light, and the smaller it was, the better. The ratio of the maximum difference value to the average value ( $\Delta/\text{Mean}$ ) could reflect the influence of the fluctuation of light intensity on the gray value. And the smaller, the better. The calculation method of the above three parameters is shown in **Figure 3c**. The results indicate type IV (a circular LED lamp with a USB interface as the exclusive light source, a confined dark space and an industrial camera to capture images) is the best shooting equipment to capture the chip image.

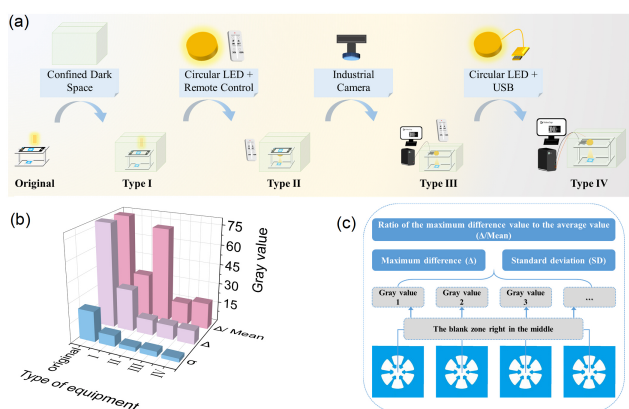


**Figure 3.** Optimization conditions for light source and shooting equipment. (a) Improvement and integration of shooting equipment; (b) The maximum difference ( $\Delta$ ) and standard deviation ( $\sigma$ ) of the gray value of the blank area of the paper-based chips when equipped with four improved equipment; (c) The calculation method of the above parameters.

All the conditions had been optimized as the best. The amount of mixed chromogenic agents added to every detection area of the chips is 2.5  $\mu\text{L}$  aliquots and the measured solution is 2  $\mu\text{L}$ . The interval between them is 10 minutes. Type IV is the best shooting equipment to capture the chip image.

### 3.3. The Calibration Detection with Standard Ni-Contained Solution

As the pH can affect the accuracy of detection, we calibrated the relationship of colorimetric VS Ni concentration at different pH (Disodium hydrogen phosphate-citrate buffer at pH = 8.0, 7.8, 7.6, 7.4, 7.2, 7.0, 6.8, 6.6), which would be beneficial for the application in the industrial park. For detection of the standard stock solution of nickel ion, the mixed chromogenic agents I of nickel ion contained 200  $\mu\text{L}$  Sodium fluoride (0.5 M), disodium hydrogen phosphate-citrate buffer and 500  $\mu\text{L}$  dimethylglyoxime (40  $\text{mg mL}^{-1}$ ), corresponding to **Figure 1**. The mixture of 2.5  $\mu\text{L}$  chromogenic agents I was dropped on six detection areas of a paper-based chip and another 2.5  $\mu\text{L}$  was dropped 10 minutes later. For another ten minutes, the standard solutions of nickel ion (1000  $\text{mg L}^{-1}$ , 900  $\text{mg L}^{-1}$ , 800  $\text{mg L}^{-1}$ , 700  $\text{mg L}^{-1}$ , 600  $\text{mg L}^{-1}$ , 500  $\text{mg L}^{-1}$ , 400  $\text{mg L}^{-1}$ , 300  $\text{mg L}^{-1}$ , 200  $\text{mg L}^{-1}$ , 100  $\text{mg L}^{-1}$ , and 50  $\text{mg L}^{-1}$ ) were added to the detection zones. The images were captured in the JPG format at 96 dpi by VideoCap of industrial cameras after the color rendering of paper-based chips at different pH values. All the results are shown in **Figure 4**. To balance out the errors in light, each paper chip was taken five times. The images were processed using ImageJ to determine the color intensity of the detection zones. The overall trend and piecewise linear relationship of the gray value of the images in **Figure 4** with concentration change for each different pH buffer is shown in **Figure 5**.

With the change of concentration, the overall trend of gray value increased until saturation. When the pH of the disodium hydrogen phosphate-citrate buffer was 6.6, nickel ions of 50  $\text{mg L}^{-1}$  almost did not show color. Regardless of the pH of the buffer solution, the naked eye could distinguish that the color of the paper chip gradually deepened as the concentration of nickel ions increased from **Figure S3**. Theoretically, the gray value increased with the concentration and saturated when the concentration reached a certain value. When the pH of the buffer was 8.0 (alkaline solution), the

gray value of the nickel ion concentration of  $700 \text{ mg L}^{-1}$  decreased slightly (**Figure 5**). When the pH of the buffer was 6.8 (acidic solution), the gray values formed a plateau at 600 and  $700 \text{ mg L}^{-1}$ . When the pH of the buffer was 7.0 (neutral solution), we considered  $1000 \text{ mg L}^{-1}$  as the saturation concentration. Below the saturation concentration, the gray value was linearly fitted to the nickel ion concentration. The relationship between saturation concentration and buffer pH is reflected in **Figure S4**. We can conclude that the saturation concentration is higher when the buffer pH is neutral, and the saturation concentration becomes lower when the buffer pH is acidic or alkaline. All the above available standard curves were 15 in total, which could meet the detection needs of various wastewater in industrial parks.

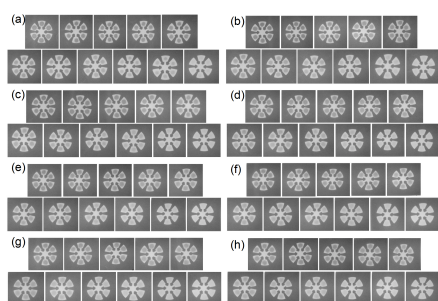


**Figure 4.** Color images of different pH buffers taken by type IV equipment. Disodium hydrogen phosphate-citrate buffer at pH = (a) 8.0; (b) 7.8; (c) 7.6; (d) 7.4; (e) 7.2; (f) 7.0; (g) 6.8; (h) 6.6.

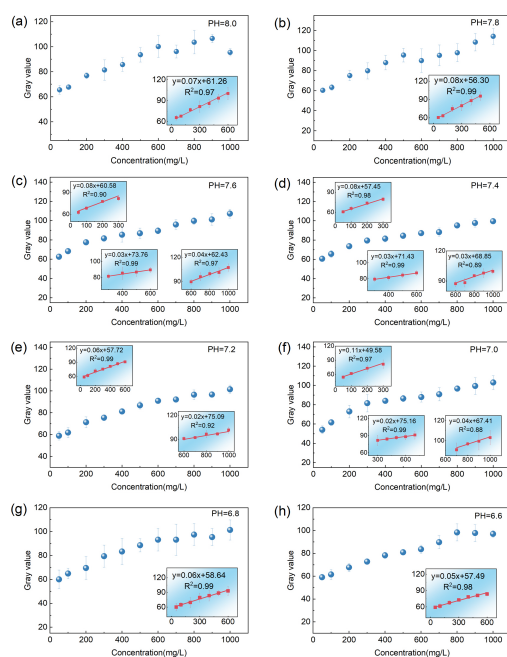


**Figure 5.** The overall trend and piecewise linear relationship of gray value with concentration change when disodium hydrogen phosphate-citrate buffer at pH = (a) 8.0; (b) 7.8; (c) 7.6; (d) 7.4; (e) 7.2; (f) 7.0; (g) 6.8; (h) 6.6.

### 3.4. Application in Detecting Real Industrial Wastewater

To test the performance of our chips on the actual wastewater detection, we carried out experiments on five typical kinds of wastewater (sample①, sample②, sample③, sample④, and sample⑤) from the Zhongshan Huafeng electroplating factory. When the pH of disodium hydrogen phosphate—citric acid buffer in the mixed chromogenic agents I was 8.0, the color of the wastewater after reacting with the mixed chromogenic agents I on the paper chip was dark in the periphery and close to white in the middle (**Figure S5**). The reason for the above phenomenon was that the composition of the wastewater was complex, where disodium hydrogen phosphate and citrate were easy to react with other components (such as  $\text{Mg}^{2+}$ ,  $\text{Ca}^{2+}$ , etc.). This could be confirmed by the color reaction of the mixed chromogenic agents I containing disodium hydrogen phosphate—citric acid buffer with the wastewater under different conditions (changing the pH or amount of buffer, adding different amounts of ammonia, etc.), as shown in **Figure S6**. Therefore, we initially used 6.3 M acetic acid and ammonia water with pH = 10.0 instead of disodium hydrogen phosphate-citrate buffer to adjust the pH. The mixed chromogenic agents were composed of  $200 \mu\text{L}$  Sodium fluoride (0.5 M),  $100 \mu\text{L}$  acetic acid solution (6.3 M),  $500 \mu\text{L}$  dimethylglyoxime ( $40 \text{ mg ml}^{-1}$ ) and  $250 \mu\text{L}$  ammonia solution (pH = 10.0). After the reaction of the mixed chromogenic agents with the wastewater, the white areas still appeared (**Figure S7**). After measuring with pH test paper preliminarily, it was found that the pH of the wastewater was close to 1 (**Figure S8**). Hence, we increased the pH of the mixed chromogenic agents (with ammonia and acetic acid) for neutralization. When the pH of the ammonia solution was 12.0, the white areas became significantly reduced in the color reaction (**Figure S9a**). When concentrated ammonia water with pH 12.6 was used, the color reaction of wastewater and mixed chromogenic agents II no longer showed white areas (**Figure S9b**). This was mainly based on the principle of acid-base neutralization. Given that the wastewater was strongly acidic, adding strong alkaline concentrated ammonia water could neutralize the hydrogen ions in the wastewater, thereby increasing the pH value of the wastewater. As the pH value of the ammonia water solution increased, from the initial pH = 10.0 to pH = 12.0, and then to pH = 12.6, the acidity in the wastewa-

ter was gradually neutralized. Correspondingly, the white area in the chromogenic reaction gradually decreased until it no longer appeared. This indicated that by adjusting the pH value, the interference of the acidic environment on the chromogenic reaction was eliminated. Consequently, the mixed chromogenic agent II could react normally with the target substances in the wastewater, thus achieving a more uniform and normal chromogenic effect. In this way, the obtained colorimetric results and the extracted gray value are repeatable and reliable.

Since the pH of wastewater was an important factor affecting colorimetry, we measured the pH of the solution with the pH meter during the test process (Figure 6a). The results showed that the pH values of sample①, sample②, sample③, and ④ were less than 2.1, and the pH values of sample⑤ were between 2.2 and 2.6. In brief, they were all strongly acidic and required neutralization by more alkaline solutions. With the increase of pH, the  $\Delta$  gray value decreased (Figure 6b), enhancing the color rendering more uniformly. Moreover, the decrease of  $\Delta$  gray value was the most significant with a pH of 12.6. Consequently, the most suitable mixed chromogenic agents for the detection of wastewater were 200  $\mu$ L Sodium fluoride (0.5 M), 100  $\mu$ L acetic acid solution (6.3 M), 500  $\mu$ L dimethylglyoxime (40 mg ml<sup>-1</sup>) and 250  $\mu$ L concentrated ammonia solution (pH = 12.6). As the pH values of various types of wastewater from the industrial park are quite different, it is difficult to control the pH value accurately based on the technique in the main text. That would have led to errors within a certain range in the measured concentration as shown in Figure 6. Further development would be to combine the analysis results with the pH value from more industrial waste to find an accurate relationship between the Ni concentration and the gray value.

After initial measurements, concentrations of sample①, sample④ and sample⑤ were believed to be below 300 mg L<sup>-1</sup>, concentrations of sample② were between 100 and 400 mg L<sup>-1</sup>, and concentrations of sample③ were between 600 and 1000 mg L<sup>-1</sup> (Figure 6c). According to the above concentration range of wastewater, the standard curves of appropriate segments were selected for calculation. The relative error between the obtained concentration calculated by different standard curves and the concentration measured by the A3 atomic absorption spectrophotometer is shown in Figure 6d,e. The most appropriate standard curve was

the one with the smallest relative error. From the first field detection in May to the second in August, we determined the dosage of all kinds of reagents, the time intervals for reaction, and the pH of ammonia used to detect industrial wastewater. Next step, we also successfully applied the type IV shooting equipment. The overall relative error of the wastewater concentration in the three tests showed a notable decreasing trend (Figure 6f). The relevant data of the third test are shown in Table 1. Those results indicated a tremendous improvement in the equipment and the optimization of various conditions, helping to obtain a smaller error with our chips.

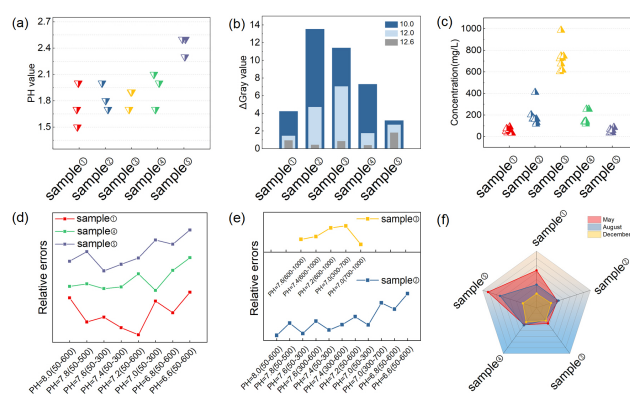


**Figure 6.** Analysis and detection of related parameters of five types of wastewater. (a) pH range of the five types of wastewater; (b) The change of the maximum value of the difference between the gray values of each detection area ( $\Delta$  gray value) caused by the different pH of ammonia in the mixed chromogenic agents; (c) Concentration ranges for five types of wastewater; (d) The relative error between the obtained concentration of wastewater (sample①, sample④ and sample⑤) and the concentration measured by the A3 atomic absorption spectrophotometer and the corresponding standard curve; (e) The relative error between the obtained concentration of wastewater (sample② and sample③) and the concentration measured by the A3 atomic absorption spectrophotometer and the corresponding standard curve; (f) Relative errors of five types of wastewater in three field tests.

All of the above data show that our paper-based chips could be put into use in practical tests in industrial parks. Given it consumed little reagent, nickel ion detection based on this technical route greatly reduced the impact of chemical reagents on the environment. In addition, since there was no necessity to dilute the wastewater in advance, the application of milli-q water was also greatly reduced. Although our technique route could meet the detection of nickel ions in industrial wastewater, the interference problem of other heavy metal ions in wastewater still needs to be solved. In

**Table 1.** The relevant data of the third field test.

Relevant Parameters	pH Range of Wastewater	pH of Disodium Hydrogen Phosphate-Citrate Buffer	Concentration Range of Wastewater	Concentration Range of Standard Curve	Concentrations Measured by Factory	Concentrations Calculated by This Work	Relative Error (%)
sample①	<2.1	7.2	<300	50–600	74.0	74.19	0.26
sample②	<2.1	8.0	100–400	50–600	160.0	183.65	14.78
sample③	<2.1	7.0	600–1000	700–1000	746.0	926.56	24.20
sample④	<2.1	7.0	<300	50–300	254.0	381.73	50.29
sample⑤	2.2–2.6	7.6	<300	50–300	57.2	59.22	3.53

Note: The units of the concentrations involved were all  $\text{mg L}^{-1}$ .

the future, we plan to study and remove substances that may cause interference.

**Table 2** summarizes the range and limitation of different methods for detecting nickel ions. From the table, our technology demonstrates a comparable detection level to other techniques for nickel ion detection. In terms of the detection range, it spans from 50 to 1000  $\text{mg L}^{-1}$ , presenting

an advantage of a relatively wider detection range compared with other methods, especially for the application in the industrial park. Compared with well-established methods such as AAS and ICP-MS, our technology is quite cheap and simple, which shows great potential in the detection of large amounts of industrial wastewater.

**Table 2.** Comparison of different methods for detecting nickel ions.

Method of Detection	Range of Detection	Limit of Detection	Ref.
Atomic absorption spectroscopy (AAS)	0.03–0.20 $\text{mg L}^{-1}$	—	2
Fluorescence spectrometer	—	14.36 nM	11
Colorimetric	0.05–100 $\mu\text{M}$	0.2 nM	12
Paper-based microfluidic platform	—	0.24 ppm	13
Inductively coupled plasma mass spectrometry (ICP-MS)	5.0–50 $\text{ng L}^{-1}$	1.32 $\text{ng L}^{-1}$	14
Electrochemical sensing platform	0.86–19.61 $\mu\text{g L}^{-1}$	0.26 $\mu\text{g L}^{-1}$	15
Preconcentration system coupled with colorimetric analysis	20–400 ppb	15 ppb	20
Microfluidic paper-based platform	2.9–1000 ppm	2.9 ppm	38
Microfluidic paper-based chips	50–1000 $\text{mg L}^{-1}$	18.5 $\text{mg L}^{-1}$	This work

## 4. Conclusions

In this study, we proposed a novel technique route to improve the stability and reliability of microfluidic paper-based chips for detecting nickel ions. To achieve those purposes, we optimized the chips (volumes of mixed chromogenic agents, the nickel ion volumes and reaction times) and the systems (the light source and camera parameters). With those improvements, we calibrated our standard text curve under different pH values (with a linear detection range of 50–1000  $\text{mg L}^{-1}$  and a lowest detection limit of 18.5  $\text{mg L}^{-1}$ ). Then, we detected five typical types of real water samples containing nickel ions from the factory. We obtained uniform colorimetric results, which indicated the reliability and repeatability of our chips and demonstrated that they could meet the daily monitoring of Ni ions in their industrial parks.

The relative errors for the five types of wastewater are 0.26%, 14.78%, 24.20%, 50.29% and 3.53%, respectively. Those results showed reliable, repeatable, and reasonable errors for five types of wastewater. The above technique route also has great potential for detecting other heavy metals in the industrial fields.

## Supplementary Materials

The following supporting information can be downloaded at <https://journals.bilpubgroup.com/public/JEES-8433-Supplementary-Materials.pdf>.

## Author Contributions

Writing—original draft, conceptualization, data curation, formal analysis, investigation, methodology, validation,

visualization, writing—review & editing, X.L.; formal analysis, methodology, Q.Y.; formal analysis, J.B. and Z.W.; supervision, writing—review & editing, X.X.; data curation, Z.N. and S.L.; supervision, S.X., C.Z. and Y.J.; funding acquisition, M.C. and D.J.; conceptualization, formal analysis, methodology, supervision, writing—review & editing, Y.Y. and J.H. All authors have read and agreed to the published version of the manuscript.

## Funding

This research was funded by the Beijing Natural Science Foundation [Grant No. Z210006] and the National Natural Science Foundation of China [Grant No. 62275061].

## Institutional Review Board Statement

Not applicable.

## Informed Consent Statement

Not applicable.

## Data Availability Statement

Data will be made available on request.

## Conflicts of Interest

The authors declare no conflict of interest.

## References

- [1] Alabssawy, A.N., Hashem, A.H., 2024. Bioremediation of hazardous heavy metals by marine microorganisms: A recent review. *Archives of Microbiology*. 206(3), 103. DOI: <https://doi.org/10.1007/s00203-023-03793-5>
- [2] Hashem, M.A., Hasan, M.A., Nayan, A.H., et al., 2021. The environmental impacts of heavy metals in soil, certain plants and wastewater near industrial area of Brahmanbaria, Bangladesh. *Environmental Monitoring and Assessment*. 193(10), 688. DOI: <https://doi.org/10.1007/s10661-021-09497-x>
- [3] Lourembam, J., Haobam, B., Singh, K.B., et al., 2024. The molecular insights of cyanobacterial bioremediations of heavy metals: The current and the future challenges. *Frontiers in Microbiology*. 15, 1450992. DOI: <https://doi.org/10.3389/fmicb.2024.1450992>
- [4] Jokić Govedarica, J., Tomašević Pilipović, D., Gvoić, V., et al., 2024. Eco-friendly nanoparticles: mechanisms and capacities for efficient removal of heavy metals and phosphate from water using definitive screening design approach. *Environmental Geochemistry and Health*. 46(4), 118. DOI: <https://doi.org/10.1007/s10653-024-01879-7>
- [5] Karthik, V., Karuna, B., Kumar, P.S., et al., 2022. Development of lab-on-chip biosensor for the detection of toxic heavy metals: A review. *Chemosphere*. 299, 134427. DOI: <https://doi.org/10.1016/j.chemosphere.2022.134427>
- [6] Mabowa, H.M., Mkhohlakali, A., Mokoena, S., et al., 2024. Removal of nickel from nickel sulfite-fire assay dissolution filtrate through precipitation. *ACS Omega*. 9(5), 5592–5600. DOI: <https://doi.org/10.1021/acsomega.3c07623>
- [7] Kumar, A., Kumar, V., Thakur, M., et al., 2023. Comprehensive review of nickel biogeochemistry, bioavailability, and health risks in the environment. *Land Degradation & Development*. 34(14), 4141–4156. DOI: <https://doi.org/10.1002/ldr.4775>
- [8] Ramadan, F., Nour, H.E., Wahed, N.A., et al., 2024. Heavy metal contamination and environmental risk assessment: a case study of surface water in the Bahr Mouse stream, East Nile Delta, Egypt. *Environmental Monitoring and Assessment*. 196(5), 429. DOI: <https://doi.org/10.1007/s10661-024-12541-1>
- [9] Serafin, J., Kishibayev, K., Tokpayev, R., et al., 2023. Functional activated biocarbons based on biomass waste for CO<sub>2</sub> capture and heavy metal sorption. *ACS Omega*. 8(50), 48191–48210. DOI: <https://doi.org/10.1021/acsomega.3c07120>
- [10] Manwani, S., Bhoot, N., Pandey, H., et al., 2022. Mitigation of lead and Cadmium from vegetable crops through different biochemical adsorbent treatments at Sanganer industrial area, Jaipur. *Materials Today: Proceedings*. 69, 1556–1564. DOI: <https://doi.org/10.1016/j.matpr.2022.07.059>
- [11] Barik, D., Anilkumar, A., Porel, M., 2024. Solid-state fluorescent organic polymers for visual detection and elimination of heavy metals in water. *ACS Polymers Au*. 4(5), 428–437. DOI: <https://doi.org/10.1021/acspolymersau.4c00048>
- [12] Fakayode, S.O., Walgama, C., Fernand Narcisse, V.E., et al., 2023. Electrochemical and colorimetric nanosensors for detection of heavy metal ions: A review. *Sensors*. 23(22), 9080.
- [13] Handa, S., Singh, P., Prakash, B., et al., 2024. Evaluation of heavy metal contamination: An analogy between conventional techniques and paper microfluidics as the futuristic probe for diverse environmental matrices. *Bulletin of Materials Science*. 47(4), 262. DOI: <https://doi.org/10.1007/s12034-024-03292-3>
- [14] Li, Y., Peng, G., He, Q., et al., 2015. Dispersive



- liquid–liquid microextraction based on the solidification of floating organic drop followed by ICP-MS for the simultaneous determination of heavy metals in wastewaters. *Spectrochimica Acta Part A: Molecular and Biomolecular Spectroscopy*. 140, 156–161. DOI: <https://doi.org/10.1016/j.saa.2014.12.091>
- [15] Fendrych, K., Porada, R., Baś, B., 2023. Electrochemical sensing platform based on Zeolite/Graphite/Dimethylglyoxime nanocomposite for highly selective and ultrasensitive determination of nickel. *Journal of Hazardous Materials*. 448, 130953. DOI: <https://doi.org/10.1016/j.jhazmat.2023.130953>
- [16] Nadumane, S.S., Biswas, R., Mazumder, N., 2024. Integrated microfluidic platforms for heavy metal sensing: A comprehensive review. *Analytical Methods*. 16(18), 2810–2823. DOI: <https://doi.org/10.1039/d4ay00293h>
- [17] Martinez, A.W., Phillips, S.T., Butte, M.J., et al., 2007. Patterned paper as a platform for inexpensive, low-volume, portable bioassays. *Angewandte Chemie. International Edition in English*. 46(8), 1318–1320. DOI: <https://doi.org/10.1002/anie.200603817>
- [18] Zhao, X., Ding, Z., Chen, H., et al., 2023. Acoustofluidics-assisted multifunctional paper-based analytical devices. *Analytical Chemistry*. 96(1), 496–504. DOI: <https://doi.org/10.1021/acs.analchem.3c04603>
- [19] Martínez-Pérez-Cejuela, H., Calabretta, M.M., Michelini, E., 2024. Chemiluminescence “add-and-measure” Sensing paper based on the prussian blue/metal–organic framework MIL-101 nanozyme for rapid hydrogen peroxide detection. *Analytical Chemistry*. 96(42), 16561–16569. DOI: <https://doi.org/10.1021/acs.analchem.4c02340>
- [20] Aryal, P., Boes, J., Brack, E., et al., 2024. Fill, fold, photo: Preconcentration and multiplex detection of trace level heavy metals in water. *ACS Sensors*. 9(10), 5479–5488. DOI: <https://doi.org/10.1021/acssensors.4c01708>
- [21] Mazur, F., Tjandra, A.D., Zhou, Y., et al., 2023. Paper-based sensors for bacteria detection. *Nature Reviews Bioengineering*. 1(3), 180–192. DOI: <https://doi.org/10.1038/s44222-023-00024-w>
- [22] Zhao, X., He, Y., Shao, S., et al., 2024. CRISPR/Cas14 and G-quadruplex DNzyme-driven biosensor for paper-based colorimetric detection of african swine fever virus. *ACS Sensors*. 9(5), 2413–2420. DOI: <https://doi.org/10.1021/acssensors.4c00090>
- [23] Ashaiba, A., Sapna, K., Arun, A.B., et al., 2024. Development and evaluation of a noninvasive microfluidic-based paper analytical device for leptospirosis diagnosis. *Analytical Chemistry*. 96(29), 11997–12005. DOI: <https://doi.org/10.1021/acs.analchem.4c01934>
- [24] Li, Y., Guo, Y., Chen, H., et al., 2024. Flexible wearable plasmonic paper-based microfluidics with expandable channel and adjustable flow rate for portable surface-enhanced raman scattering sweat sensing. *ACS Photonics*. 11(2), 613–625. DOI: <https://doi.org/10.1021/acsphotonics.3c01490>
- [25] Steijlen, A.S.M., Parrilla, M., Van Echelpoel, R., et al., 2023. Dual microfluidic sensor system for enriched electrochemical profiling and identification of illicit drugs on-site. *Analytical Chemistry*. 96(1), 590–598. DOI: <https://doi.org/10.1021/acs.analchem.3c05039>
- [26] Campu, A., Muresan, I., Craciun, A.-M., et al., 2023. Innovative, flexible, and miniaturized microfluidic paper-based plasmonic chip for efficient near-infrared metal enhanced fluorescence biosensing and imaging. *ACS Applied Materials & Interfaces*. 15(48), 55925–55937. DOI: <https://doi.org/10.1021/acsami.3c08658>
- [27] Wu, H., Chen, J., Lin, P., et al., 2024. Nanozyme-catalyzed colorimetric detection of the total antioxidant capacity in body fluids by paper-based microfluidic chips. *ACS Applied Materials & Interfaces*. 16(30), 39857–39866. DOI: <https://doi.org/10.1021/acsami.4c07835>
- [28] Singh, S., Raucci, A., Cimmino, W., et al., 2024. Paper-based analytical devices for cancer liquid biopsy. *Analytical Chemistry*. 96(9), 3698–3706. DOI: <https://doi.org/10.1021/acs.analchem.3c04478>
- [29] Xu, B., Ding, Y., 2022. Hydrophilic/hydrophobic SiO<sub>2</sub> nanoparticles enabled janus-type paper through commercial glaco spraying and air-plasma treatment. *Advanced Materials Interfaces*. 9(21), 2200934. DOI: <https://doi.org/10.1002/admi.202200934>
- [30] Cao, Y., Sun, Y., Yu, R.-J., et al., 2023. Paper-based substrates for surface-enhanced Raman spectroscopy sensing. *Microchimica Acta*. 191(1), 8. DOI: <https://doi.org/10.1007/s00604-023-06086-2>
- [31] Romanholo, P.V.V., de Andrade, L.M., Silva-Neto, H.A., et al., 2024. Digitally controlled printing of bioink barriers for paper-based analytical devices: An environmentally friendly one-step approach. *Analytical Chemistry*. 96(14), 5349–5356. DOI: <https://doi.org/10.1021/acs.analchem.3c03801>
- [32] Filippidou, M.-K., Chatzandroulis, S., 2023. Microfluidic devices for heavy metal ions detection: A review. *Micromachines*. 14(8), 1520. DOI: <https://doi.org/10.3390/mi14081520>
- [33] Kulkarni, R.M., Sunil, D., 2024. Small molecule optical probes for detection of H<sub>2</sub>S in water samples: A review. *ACS Omega*. 9(13), 14672–14691. DOI: <https://doi.org/10.1021/acsomega.3c08573>
- [34] Zhang, Y., Yu, Y., Yang, X., et al., 2024. Pb(II) inhibits CRISPR/Cas12a activation and application for paper-based microfluidic biosensor assisted by smartphone. *Sensors and Actuators B: Chemical*. 398, 134732. DOI: <https://doi.org/10.1016/j.snb.2023.134732>
- [35] Fan, K., Zeng, J., Yang, C., et al., 2022. Digital quantification method for sensitive point-of-care detection of salivary uric acid using smartphone-



- assisted  $\mu$ PADs. *ACS Sensors*. 7(7), 2049–2057. DOI: <https://doi.org/10.1021/acssensors.2c00854>
- [36] Yang, R., Cheng, W., Chen, X., et al., 2018. Color space transformation-based smartphone algorithm for colorimetric urinalysis. *ACS Omega*. 3(9), 12141–12146. DOI: <https://doi.org/10.1021/acsomega.8b01270>
- [37] Lin, Y., Ye, S., Tian, J., et al., 2023. Paper-assisted ratiometric fluorescent sensors for on-site sensing of sulfide based on the target-induced inner filter effect. *Journal of Hazardous Materials*. 459, 132201. DOI: <https://doi.org/10.1016/j.jhazmat.2023.132201>
- [38] Chaiyo, S., Kunpatee, K., Kalcher, S., et al., 2024. 3D Paper-Based Device Integrated with a Battery-Less NFC Potentiostat for Nonenzymatic Detection of Cholesterol. *ACS Measurement Science Au*. 4(4), 432–441. DOI: <https://doi.org/10.1021/acsmesureciau.4c00012>
- [39] Xiong, X., Guo, C., Yan, G., et al., 2022. Simultaneous Cross-type Detection of Water Quality Indexes via a Smartphone-App Integrated Microfluidic Paper-Based Platform. *ACS Omega*. 7(48), 44338–44345. DOI: <https://doi.org/10.1021/acsomega.2c05938>